minerals

MDPI

Article

Sorption of Differently Charged Gold Nanoparticles on Synthetic Pyrite

Suxing Luo [1,2], Xin Nie [1], Meizhi Yang [1,2], Yuhong Fu [3], Ping Zeng [1,2] and Quan Wan [1,*]

[1] State Key Laboratory of Ore Deposit Geochemistry, Institute of Geochemistry, Chinese Academy of Sciences, Guiyang 550081, China; luosuxing123123@163.com (S.L.); niexin2004@163.com (X.N.); yangmeizhi@mail.gyig.ac.cn (M.Y.); zengpeng@mail.gyig.ac.cn (P.Z.)

[2] University of Chinese Academy of Sciences, Beijing 100049, China

[3] School of Geographic and Environmental Sciences, Guizhou Normal University, Guiyang 550001, China; fuyuhong_gznu@163.com

* Correspondence: wanquan@vip.gyig.ac.cn; Tel.: +86-0851-85891928

Received: 10 August 2018; Accepted: 25 September 2018; Published: 29 September 2018

Abstract: Sorption of nanoparticles on mineral surfaces has been well recognized for its environmental implication. For certain gold ore deposits, sorption of gold nanoparticles (AuNPs) on pyrite may constitute a critical step in the metallogenesis process, yet it has not been adequately investigated. In this work, we synthesized negatively charged, positively charged AuNPs and pyrite respectively, and experimentally studied sorption of AuNPs on pyrite in an anaerobic environment. The effects of AuNPs charge characteristics, pH, hexadecyl trimethyl ammonium bromide (CTAB) concentration, and ionic strength were evaluated. For the negatively charged AuNPs, almost no sorption was observed owing to the electrostatic repulsion between the AuNPs and pyrite surface (with a measured isoelectric point of 2.0). In contrast, positively charged AuNPs could be significantly adsorbed on pyrite through electrostatic attraction, with the sorption extent decreasing with the increase of pH (2.2–9.1). However, the adsorption of CTAB from the solution was found to increase with the increase of pH. Furthermore, deliberately added CTAB seemed to inhibit the sorption of AuNPs. Our study not only demonstrates that the electrostatic interaction is the dominant mechanism in the sorption of AuNPs on pristine pyrite, but also reveals the important competitive relation between AuNPs and CTAB in the sorption process.

Keywords: gold nanoparticles; pyrite; sorption; charge; electrostatic interaction

1. Introduction

Natural nanoparticles have been commonly found throughout the earth system [1]. Meanwhile, engineered nanoparticles have been increasingly manufactured and used over the last several decades, reaching a global production of over 260,000–309,000 metric tons in 2010 [2,3]. By estimation, a vast majority amount of the manufactured nanomaterials will be released into the environment via various pathways during their life cycles [3]. Such a large amount of natural and engineered nanoparticles would very likely interact with ubiquitous minerals in the environment [4]. Among various interactions, sorption between nanoparticles and minerals may play a critical role in the transport, fate, and exposure route of nanoparticles, and can consequently affect their occurrence state, potential toxicity as well as geochemical cycling of associated elements [4,5]. Therefore, much recent work has been devoted to the sorption of nanoparticles on various kinds of mineral surfaces, including sulfide minerals [6], clay particles [7], hematite colloids [8], mica [9], calcium carbonate sand [10], etc.

Among metallic nanoparticles, gold nanoparticles (AuNPs) are of particular interest owing to their unique properties and widespread applications in the fields of catalysis, chemical, and biological

sensing, etc. [11]. In order to assess the environmental implication of engineered AuNPs, experimental methods and theoretical models have been developed to quantify their concentrations in different environmental media (e.g., soil, water) as well as the likelihood of their potential exposure to ecosystem receptors [12,13]. Since sorption of AuNPs on mineral surfaces can substantially modify the surface properties of mineral grains, such a process undoubtedly deserves careful attention in many relevant mineralogical and environmental scenarios [14]. In addition, natural AuNPs, usually referred to as "invisible gold", have been found in several hydrothermal and supergene ore deposits of outstanding economic importance, for example, in Carlin-type gold deposits, where AuNPs are mainly hosted in pyrite [15–17]. Since the discovery of Carlin-type gold deposits half a century ago, extensive efforts have been devoted to determining the concentration, structure, morphology, and properties of the Au species in ore samples [16]. Yet, a comprehensive metallogenesis of these gold deposits remains poorly understood [18,19]. Particularly, despite a few existing theories on the formation and transport of AuNPs, a commonly accepted mechanism for the occurrence state of AuNPs is still not available [17,20]. Although it is still debatable whether AuNPs is a form of gold transportation, a consequence of the metallogenic process, or both, the interaction between AuNPs and pyrite (very likely through sorption) clearly constitutes a key element in the microscopic metallogenic mechanism [15,16].

Nevertheless, so far only a very limited number of studies have explored the sorption of AuNPs on the surfaces of sulfide minerals. Mikhlin et al. [6] pioneered the investigation of deposition of gold species on natural pyrite and found that both Au (III) and AuNPs could be deposited on pyrite. Using electrochemical techniques, Eghbalnia et al. [21] confirmed sorption of AuNPs on pyrite from colloidal solutions. Being aware of easy oxidation of pyrite exposed to air or water [22], Fu et al. [23] experimentally demonstrated that pyrite oxidation could promote sorption of negatively charged AuNPs. All these studies used natural pyrite, which might complicate the sorption of AuNPs due to inevitable variations in crystalline surfaces and impurities [24]. Furthermore, few results were obtained from sorption experiments under anaerobic condition, and the effects of solution parameters including pH, ionic strength, and ligand of AuNPs were not adequately evaluated.

In order to improve our understanding of the AuNPs-pyrite sorption behavior, we have systematically investigated the effects of experimental conditions on the sorption of AuNPs on synthetic pyrite under anaerobic condition. Because of the apparent importance of electrostatic interactions [25], we also compared the sorption results using both negatively and positively charged AuNPs, which to our knowledge has not been reported in previous studies. Our findings are expected to provide important clues to certain metallogenic processes of gold deposits and promote a better understanding of the interactions between nanoparticles and sulfide minerals.

2. Materials and Methods

2.1. Reagents

Chloroauric acid tetrahydrate ($HAuCl_4 \cdot 4H_2O$) (≥99.9%) was purchased from Shanghai Jiuyue Chemical Co., Ltd. (Shanghai, China). Sodium citrate (≥99.0%) was purchased from Shanghai Shenbo Chemical Co., Ltd. (Shanghai, China). Hexadecyl trimethyl ammonium bromide (CTAB) (≥99.0%), sodium sulfide ($Na_2S \cdot 9H_2O$) (≥99.0%), ferrous sulfate ($FeSO_4 \cdot 7H_2O$) (≥99.0%), sulfur (S) (≥99.0%), hydrochloric acid (HCl) (36~38%), nitric acid (HNO_3) (65~68%), sodium chloride (NaCl) (≥99.0%), sodium hydroxide (NaOH) (≥99.0%), sodium borohydride ($NaBH_4$) (≥99.0%), L (+)-ascorbic acid (L-AA) (≥99.0%), and ethanol (C_2H_5OH) (≥99.7%) were purchased from Sinopharm Chemical Reagent Co., Ltd. (Shanghai, China). All chemicals were of analytical or guaranteed reagent grade and were used without further purification. Deionized water was obtained from a Millipore synergy UV system (resistivity, 18.2 MΩ•cm, Millipore corporation, Molsheim, Alsace, France). Before use, all glassware and magnetic stirrers were thoroughly soaked in aqua regia (HCl/HNO_3 = 3:1, *V*/*V*), and then rinsed with copious amounts of deionized water. Gold colloids were prepared as discussed in Section 2.2. Samples of gold colloids were deoxygenated by bubbling argon gas (99.999%) for at least 5 h and then

stored in vacuum for at least 32 h in an anaerobic chamber (855-ACB, PLAS-LABS INC., Lansing, MI, USA; 10% H_2 in Ar with Pd catalyst).

2.2. Synthesis and Characterization of Gold Colloids

Negatively charged AuNPs were synthesized using the Frens method [26]. Briefly, 10.5 mL of sodium citrate solution (1.00%, *w*/*w*) was quickly added to 300 mL of boiling $HAuCl_4$ solution (0.01%, *w*/*w*) and then stirred for 25 min. After the reaction mixtures changed to a wine-red color, the samples were cooled down to ambient temperature and stored in a refrigerator at 4 °C.

Positively charged AuNPs were synthesized using a seed-mediated method [27,28]. First, 0.05 mL of 2.4×10^{-2} mol/L $HAuCl_4 \cdot 4H_2O$ was added in 3.45 mL of 0.1 mol/L CTAB solution. The color of the mixture quickly changed from light yellow to orange [29]. Then, 1.5 mL of 0.01 mol/L ice-cold $NaBH_4$ was added in the mixture. After being vigorously mixed for about 30 s, the mixture became light brown and would be used as seeds for further synthesis of AuNPs after 2 h of aging at 25 °C. Second, to prepare the growth solution, 0.08 mL of 0.2 mol/L CTAB and 0.08 mL of 2.4×10^{-2} mol/L $HAuCl_4 \cdot 4H_2O$ were mixed with 9.4 mL of H_2O. Subsequently, 0.6 mL of 0.10 mol/L freshly prepared L-AA was gently mixed with the above mixture, which immediately turned from orange to colorless. Then, 50 µL of the 2 h-aged Au seed solution was added into the colorless growth solution and blended vigorously for 20 s, and the resulting mixture turned red gradually. After standing without disturbance for 24 h at 25 °C, the above mixture was centrifuged and re-dispersed three times to remove excessive CTAB.

The morphology of AuNPs was characterized using a transmission electron microscope (TEM, Tecnai G2 F20 S-Twin, FEI Company, Hillsboro, OR, USA) and the particle size was analyzed using the Image J (US National Institutes of Health, Version 1.48, Bethesda, MD, USA) software. The zeta potentials of AuNPs were determined using a Malvern Zetasizer (Nano ZS90, Malvern, UK). Five repeats for each sample were conducted in the measurements.

2.3. Synthesis, Characterization, and Pretreatment of Pyrite

Pyrite was synthesized according to the literature [30]. Briefly, 0.02 mol of $FeSO_4 \cdot 7H_2O$ and 0.02 mol of $Na_2S \cdot 9H_2O$ were mixed in 40 mL of deionized water and black precipitate appeared immediately. Then 0.02 mol of $Na_2S \cdot 9H_2O$ and 0.02 mol of S were dissolved into 30 mL of deionized water and heated until the solution became transparent. After that, the suspensions prepared above were added into a 150 mL Teflon-lined stainless autoclave. With the pH adjusted to pH 12.0 by adding 1 mol/L HCl, the above mixture was maintained at 433 K for 24 h. After cooling to room temperature, the resulting black product was collected via centrifugation (5000 rcf), washed several times with 1 mol/L H_2SO_4 to remove the residual FeS, then added into 0.1 mol/L Na_2S boiling solution to remove the sulfur, and finally washed with absolute ethanol or water to remove residual salts. The product was subsequently dried in a vacuum oven (DZF-6050, Shanghai Shenxian Thermostatic Equipment, Shanghai, China) at 60 °C for 5 h, and characterized by X-ray diffraction (XRD, Empyrean, PANalytical B.V, Almelo, The Netherlands) (Figure S1) operating with Cu-Kα radiation. The size and morphology of the product was examined by scanning electron microscopy (SEM, Scios, FEI Company, Hillsboro, OR, USA) (Figure S2) with an acceleration voltage of 30.0 kV.

To remove oxidized surface species, the pyrite sample was immersed in 3 mol/L HCl for 3 h with ultrasonication (BL10-300C, Shanghai Bilon Experiment Eqipment Co., Ltd., Shanghai, China), then washed ten times with ethanol, and dried overnight under vacuum [31]. To verify the cleaning efficiency, 0.02 g of pyrite was stirred in 16 mL of de-oxygenated water (same solid/liquid ratio as that of the sorption system) for 1 h. The suspension was filtered through a membrane (0.1 µm pore size) and the concentration of iron in the supernatant was measured by Atomic Absorption Spectroscopy (AAS, 990SUPER, Beijing Purkinje General Instrument Co., Ltd., Beijing China; detection limit 0.01 ppm) with an excitation wavelength of 248.3 nm. After the acid-cleaning pretreatment, the iron concentration in

the supernatant was less than 0.01 ppm indicating that nearly complete removal of oxidation products. To ensure oxidation-free pyrite surface, pyrite was freshly pretreated before each sorption experiment.

The zeta potentials of pyrite samples were obtained by electrophoretic effect using a Zetasizer (DelsaNanoC, Beckmancoulter, Brea, CA, USA). The NaCl was used to maintain the ionic strength at 10^{-3} mol/L [32]. Each sample was measured three times to get the average zeta potential value.

2.4. Sorption and Desorption Experiments

All sorption and desorption experiments were conducted in a glove box filled with 90% Ar, 10% H_2, and with the presence of Pd catalyst at room temperature. The initial pHs of the Au colloids were adjusted in the range of 2.2–10.0 using 2 mol/L HCl or NaOH solutions. The concentration of CTAB in the Au colloids was changed in order to investigate its effect on the sorption behavior. The ionic strengths of the Au colloids were controlled by adding different amount of NaCl, whose final concentrations were maintained at 0, 0.005, 0.01 mol/L, respectively. In a typical sorption experiment, 0.04 g of pyrite and 32 mL of 22 ppm Au colloid was added into a 40-mL sealed glass bottle. The suspension was agitated using a magnetic stirrer with a stirring speed of 300 rpm throughout the experiment. At selected time intervals, 1.5 mL of the suspension was sampled and centrifuged for 5 min (4000 rcf). Then, 1 mL of the resulting supernatant was digested overnight with 1 mL of aqua regia to analyze the Au concentration using AAS (990SUPER, Beijing Purkinje General Instrument Co., Ltd., Beijing, China; detection limit 0.1 ppm). The extent of sorption was determined based on the difference in Au concentration between initial and final liquid phases. Additionally, the CTAB concentrations in the filtered solutions were determined based on the color fading of methyl orange with CTAB using a UV-vis spectrophotometer [33] (UV-vis, CARY 300, Agilent, Santa Clara, CA, USA). The sodium citrate concentrations were determined using a liquid chromatographer equipped with a standard micro auto sampler (HPLC, Agilent1200, Agilent, Santa Clara, CA, USA). A small fraction of the pyrite solid separated from centrifugation was characterized by SEM (SCIOS, FEI Company, Hillsboro, OR, USA).

The desorption experiments were carried out by stirring (300 rpm) pyrite separated (centrifugation: 4000 rcf, 5 min) from the sorption suspension in de-oxygenated water with 0, 23.6 ppm, 50 ppm of CTAB at pH 3.0. The solid/liquid ratio was maintained at the same level of the sorption suspension. Similar to the sorption experiment, the gold concentration in the liquid phase and the morphology of the solid were characterized using AAS and SEM, respectively.

3. Results and Discussion

3.1. Characterization of Synthesized AuNPs and Pyrite

(a) Negatively charged AuNPs. The morphology and size distribution of the negatively charged AuNPs were examined by TEM. As shown in Figure 1a, most AuNPs were spherical or ellipsoidal, with an average size of about 18.2 nm based on the statistical analysis of more than 100 particles in the TEM images using the ImageJ software. Zeta potential, the effective surface potential at the hydrodynamic "shear plane", provides important information about the charge carried by the nanoparticles. A particle suspension with an absolute value of zeta potential less than 20 mV (in the absence of other stabilizing factors) is usually considered to be unstable and may result in particle aggregation [34]. The AuNPs synthesized by the Frens method showed negative surface potentials at all tested pH conditions due to citrate adsorption on the particle surface (Figure 2a). Because of the dissociative property of citric acid (a triprotic acid) [35], the surface charge and thus the zeta potential of AuNPs became generally more negative at higher pH. At pH over 7.0, the absolute value of the zeta potential appeared to decrease, possibly caused by the charge regulation effect originated from the electrostatic repulsion among neighboring highly charged citrate species. Nevertheless, the high absolute values (>20 mV) in the pH range of 4.0–10.0 indicate reasonable stability against aggregation.

(b) Positively charged AuNPs. Most of the positively charged AuNPs were spherical or ellipsoidal in shape (Figure 1b) with the average size of 14.4 nm. Since CTAB is a cationic surfactant with a positive ammonium head group [36], the CTAB-capped AuNPs always carry positive charges over the pH range studied (Figure 2b). The absolute zeta potential value showed a decreasing trend with the increase of pH, reaching 50.8 mV at pH 2.3 and 22.9 mV at pH 11.0, respectively. This pH dependence is likely due to the screening effect of hydroxide anions coming close to the ammonium head group. Good colloidal stability (for at least 180 days) of the positively charged AuNPs over the whole pH range was indicated based on visual observation and UV-Vis absorbance measurement (e.g., Figure S3).

(c) Pyrite. Pyrite was synthesized based on a literature method [30]. Figure S1 shows the XRD pattern of the synthetic iron disulfide, with the main diffraction peaks easily indexed to a pure-phase pyrite (JCPDS No. 42–1340). The pyrite particles exhibit a cubic shape and the average particle size was about 650 nm (Figure S2). Zeta potential measurements for our pyrite samples under anaerobic conditions (Figure 3) indicate an isoelectric point of 2.0, which suggests pyrite carried negative surface charges under most of our experimental conditions (pH > 2.0). Besides, this isoelectric point value is in agreement with those found in earlier studies [37], which further implies our pyrite (after acid pretreatment) was not oxidized.

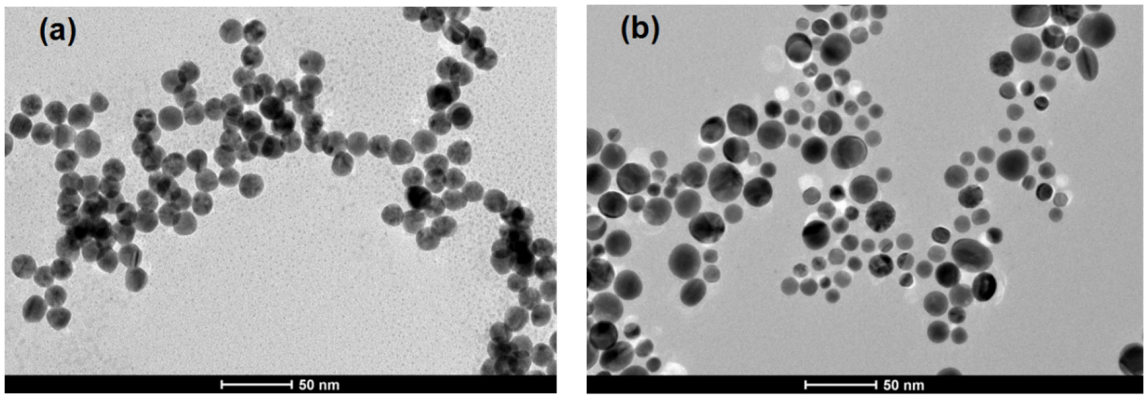

Figure 1. TEM micrographs of the differently charged gold nanoparticles (AuNPs): (**a**) negatively charged AuNPs; (**b**) positively charged AuNPs.

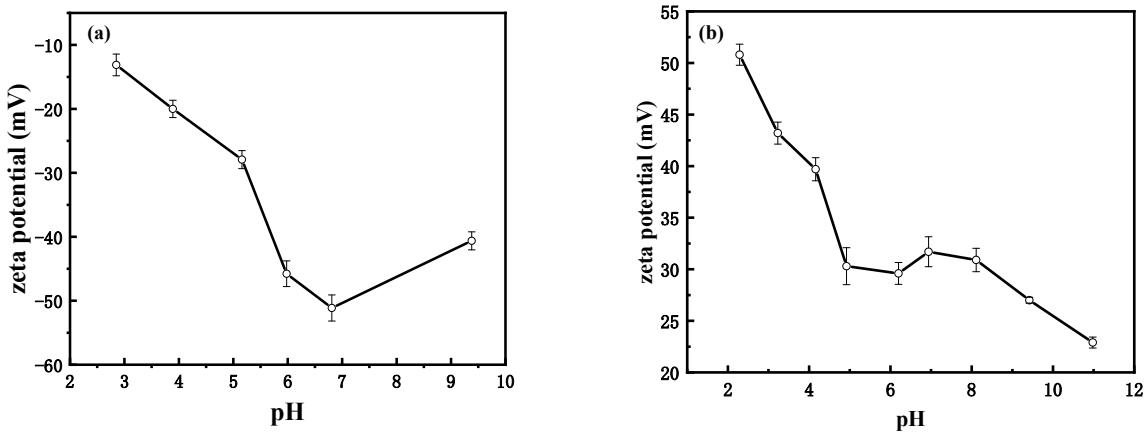

Figure 2. Zeta potentials of the differently charged AuNPs: (**a**) negatively charged AuNPs; (**b**) positively charged AuNPs.

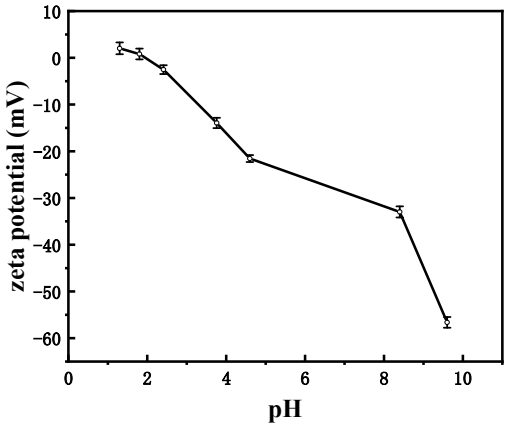

Figure 3. Zeta potentials of synthesized pyrite.

3.2. *Effect of AuNPs Charge Characteristics on Sorption Behaviors*

For sorption experiments using negatively charged AuNPs under pH range 4.0–10.0, Au concentration in the liquid phase remained almost unchanged even after prolonged stirring time (up to 168 h), which suggests negligible sorption of AuNPs on the pyrite surface. Accordingly, almost no AuNPs could be found in the SEM image (Figure 4) of pyrite after sorption with negatively charged AuNPs for 168 h (pH = 4.0). In the Frens method, to prepare our negatively charged AuNPs (with a 4.65:1 citrate/$HAuCl_4$ molar ratio), citrate functioned as both reducing and stabilizing agent and a considerable amount of citrate (292–300 mg/L) existed in the final gold colloids. The approximately constant concentration of citrate (measured by HPLC) in the liquid phase also suggests little adsorption of citrate ligand by pyrite. According to the classic Derjaguin-Landau-Verwey-Overbeek (DLVO) theory, the total potential energy in a sorption system consists of van der Waals attraction and electrical double layer interaction. As discussed in Section 3.1, since pyrite and citrate-capped AuNPs both carry negative charges under our experimental condition, it seems straightforward to imagine the repulsive electrostatic interaction between them. Nevertheless, our work serves as a convincing evidence to demonstrate that such an electrostatic repulsion is strong enough to generate a substantial energy barrier preventing any significant sorption of negatively charged AuNPs on pyrite surface.

Although some previous studies did report significant sorption of negatively charged AuNPs on pyrite [6,23], it has to be recognized that the pyrite surfaces of these studies were subject to different extent of oxidation, which shifted the isoelectric point to a higher value (e.g., $pH_{iep} \geq 6$). At pH < pHiep, the oxidized pyrite would bear positive surface charges which led to favorable condition for the sorption of negatively charged AuNPs through electrostatic attraction [38].

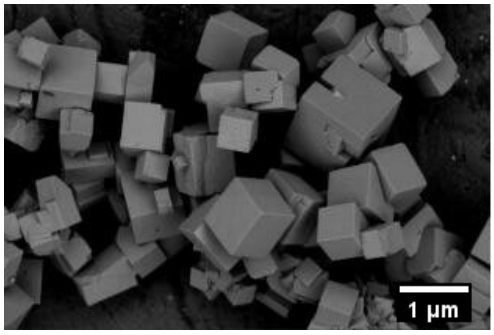

Figure 4. SEM image of pyrite after sorption with negatively charged AuNPs for 72 h (pH = 4.0).

For positively charged AuNPs, Figure 5 presents the relative residual concentration of AuNPs in the supernatant as a function of sorption time at different pHs. In contrast to negatively charged AuNPs, positively charged AuNPs could be adsorbed by pyrite, especially under acidic conditions.

Specifically, the nearly zero relative residual concentration at pH 2.2–3.0 indicates almost complete sorption of AuNPs within 29 h, while partial sorption occurs at higher pH. At pH 9.1, only about 3.5% of positively charged AuNPs were adsorbed on pyrite even after 48 h of adsorbing time. The larger sorption of positively charged AuNPs (in contrast to negatively charged AuNPs) was obviously due to the electrostatic attraction between positively charged AuNPs and negatively charged pyrite surface. However, simple electrostatic interaction could not easily account for the pH dependence of the sorption, because as the pH increased, decreasing zeta potentials of AuNPs (Figure 2b) resulted in less electrostatic attraction with pyrite, while on the contrary, increasing absolute value of zeta potentials of pyrite (Figure 3) led to larger electrostatic attraction. We suspect that the observed pH dependence might involve the competitive adsorption of positively charged AuNPs (i.e., CTAB-capped AuNPs) and CTAB cations (hexadecyl trimethyl ammonium) on pyrite surface, and thus simultaneously measured the adsorption of CTAB as a function of pH. As shown in Figure 6, the concentration of the residual CTAB in the sorption system decreased with the increasing pH, corresponding to increased adsorption of CTAB perhaps due to the increased absolute value of zeta potential of pyrite (thus increased electrostatic attraction). The roughly opposite pH dependences reflected in Figures 5 and 6 are compatible with the presumed mechanism of competitive adsorption. Specifically, as the pH increases, CTAB cations become preferentially adsorbed on pyrite surface, which not only occupy more adsorbing sites of pyrite and but also exert electrostatic repulsion to the approaching AuNPs.

It should be noted that a dramatic increase in the sorption of positively charged AuNPs was observed when the pH was further increased to 10.0, despite the larger adsorption of the competing CTAB cations. We speculate this result might be mainly caused by the increased ionic strength (further discussed in Section 3.4) as well as more negative charges on the surface of pyrite at this pH.

The pH dependence of sorption of positively charged AuNPs was further verified by SEM. Figure 7 shows the SEM images of pyrite after sorption of positively charged AuNPs at different pHs for 48 h, while the corresponding XPS data (e.g., Figure S4) confirm the existence of Au element on the pyrite surface. As can be seen, numerous AuNPs were adsorbed on the surface of pyrite at pH 2.2, while the number of adsorbed particles decreased with the increase of pH. At pH > 7.0 (especially at pH 10.0), many AuNPs appeared to exist in the form of homoaggregation, consistent with the effect of increased ionic strength due to added sodium hydroxide when adjusting pH from initially 3 to 7 or above.

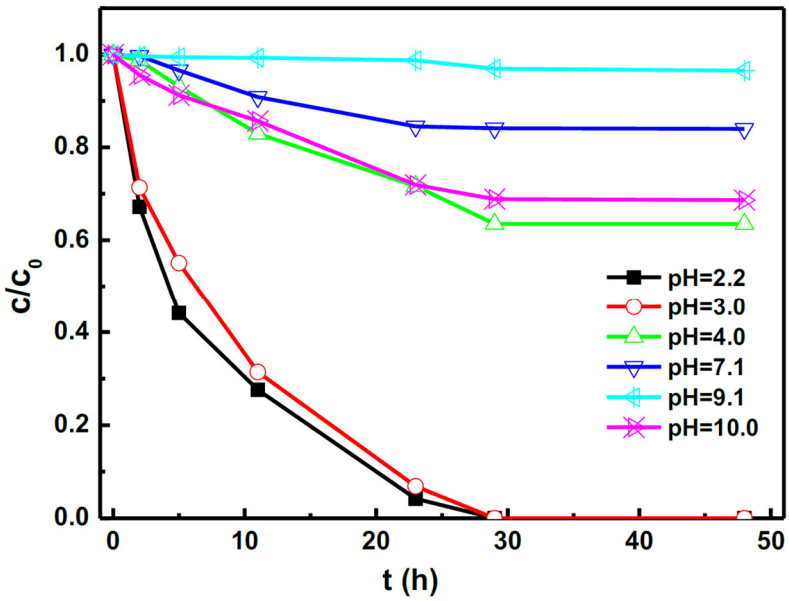

Figure 5. AuNPs sorption behavior on pyrite surface as a function of pH.

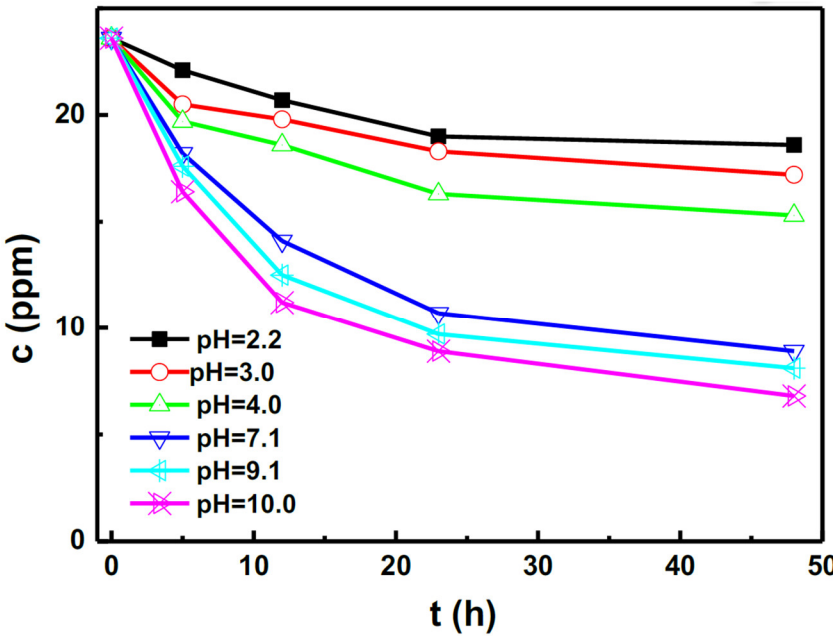

Figure 6. The residual hexadecyl trimethyl ammonium bromide (CTAB) after sorption as a function of pH.

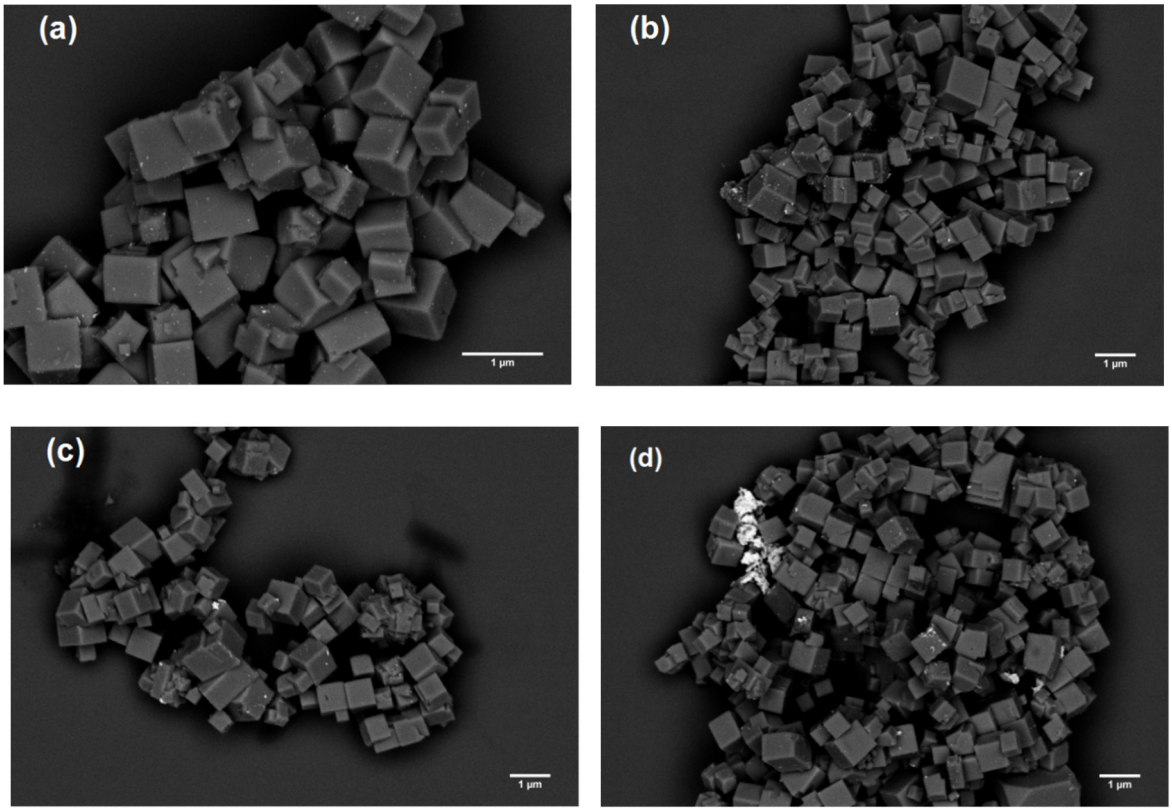

Figure 7. SEM images of pyrite after sorption with positively charged AuNPs at different pHs (**a**) pH = 2.2; (**b**) pH = 4.0; (**c**) pH = 7.1; (**d**) pH = 10.0.

3.3. Effect of CTAB Concentration on the Sorption of Positively Charged AuNPs

To further investigate the competing role of CTAB, we deliberately added CTAB in the sorption system at pH 3.0, where positively charged AuNPs should be almost completely adsorbed by the pyrite within 29 h (Figure 5). The concentration of CTAB was controlled from 23.6 (the original concentration

without any addition) to 200 ppm. As shown in Figure 8, nearly full sorption of AuNPs (i.e., C/C_0 reaching zero) by pyrite could be achieved with CTAB concentration of ranging from 23.6 to 100 ppm. However, the time needed to reach any lowered C/C_0 value apparently increased with the increase of CTAB concentration, indicating decreased adsorption speed of AuNPs through CTAB addition. When the CTAB concentration was further increased to 150 (or 200) ppm, only approximately 36.6% (or 23.4%) of AuNPs could be adsorbed by pyrite even after 100 h of sorption time.

All these results (Figures 5, 6 and 8) support the competitive relation between CTAB and positively charged AuNPs, despite their dramatic difference in length scale. The much smaller CTAB molecules should diffuse faster than AuNPs, and in this sense are kinetically advantageous in competing for adsorbing sites on pyrite. The pre-adsorbed CTAB could on the one hand occupy active sites on the surface of pyrite, on the other hand repel the approaching AuNPs electrostatically and sterically, thus exhibiting a strong competing behavior against the sorption of AuNPs. Such a mechanism of competitive sorption may be generally applicable to many superficial or supergene environments where organic ligands are abundant in the fluids, and therefore profoundly affect the sorption and ultimately the transport and fate of NPs.

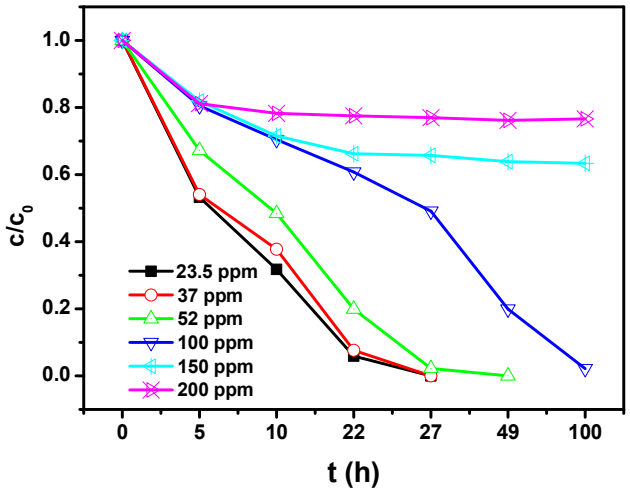

Figure 8. Effect of CTAB concentration on the sorption of positively charged AuNPs.

3.4. Effect of Ionic Strength on the Sorption of Positively Charged AuNPs

Ionic strength (or salinity) is known to strongly affect the aggregation and sorption behaviors of nanoparticles [39,40]. To elucidate the effect of ionic strength on the sorption of AuNPs, we have conducted sorption experiments with increased NaCl concentrations (through addition of salt) at pH 4.0 and 7.1, respectively. Under such pH conditions, incomplete sorption of AuNPs would occur if without the addition of NaCl. For example, even after 48 h of sorption, only 36.3% and 16.0% of AuNPs were absorbed on pyrite surface at pH 4.0 and 7.1, respectively (see Figure 5). In contrast, as shown in Figure 9, the sorption speed and sorption capacity of positively charged AuNPs on pyrite increased significantly with the addition of NaCl at both pHs. At 0.01 mol/L concentration of added NaCl, almost full sorption of AuNPs was observed at pH 4.0 (27 h) and 7.1 (53 h), respectively. The effect of increased salinity on the sorption process is explained as follows. First, the increased ionic strength will considerably lower the absolute values of the zeta potentials for both AuNPs and pyrite (as evidenced in Figures S5–S8) because of the compression of electric double layers. Thus, according to the DLVO theory, the increase in ionic strength may screen not only electrostatic attraction between AuNPs and pyrite, but also electrostatic repulsion among charged AuNPs [41,42]. Therefore, the repulsive interaction between adsorbed AuNPs on pyrite and approaching AuNPs from the suspension can be reduced, which favors an increase of the sorption extent. Second, perhaps more importantly, higher ionic strength and thus lowered electrostatic repulsion may also induce different degrees of homoaggregation among AuNPs, which was supported by the gradual color change from red to

purple and SEM observations (not shown). In other words, attractive van der Waals interactions may become a dominant force [10], which leads to higher extent of homoaggregation and also sorption of AuNPs.

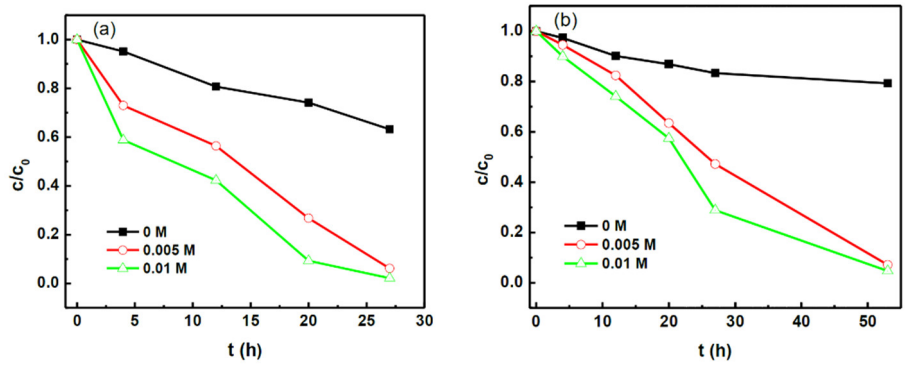

Figure 9. Effect of ionic strength on the sorption of positively charged AuNPs on pyrite (**a**) pH = 4.0; (**b**) pH = 7.1.

3.5. Desorption of Positively Charged AuNPs

Desorption experiments were conducted by stirring (300 rpm) pyrite separated from sorption suspension in a solution (pH 2.2) containing 0, 23.6, or 50 ppm CTAB, respectively. Irrespective of the CTAB concentration, after stirring for up to 168 h, no AuNPs were detected in the supernatant. Nevertheless, SEM images (e.g., Figure 10) indicate that most AuNPs were desorbed and mainly existed as homo-aggregates. The result suggests that the interaction between AuNPs and pyrite is probably not very strong, which allows desorption of AuNPs after long duration of stirring. Further work is needed to elucidate the exact mechanism.

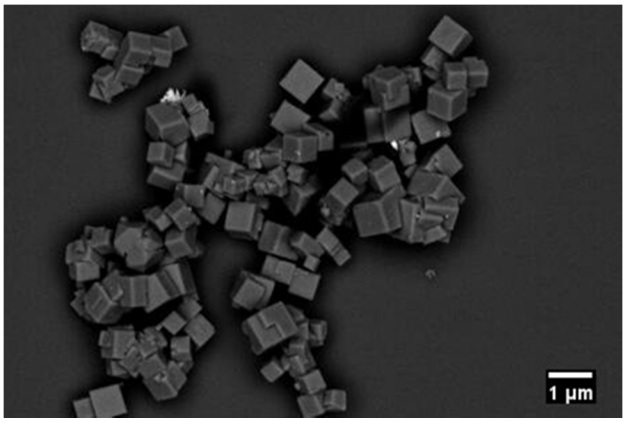

Figure 10. SEM image of pyrite after desorption experiment in a solution of 50 ppm CTAB.

4. Conclusions

Sorption of differently charged AuNPs on synthesized pyrite has been systemically investigated in an anaerobic atmosphere. Under our experimental condition, virtually no adsorption of negatively AuNPs could be detected at pH 4.0 to 10.0. However, positively charged AuNPs could be significantly adsorbed on pyrite surface, with the extent of sorption decreasing from 100% at pH 2.2–3.0 to 3.5% at pH 9.1. In contrast, the adsorption of CTAB on pyrite increased with the increase of pH, and deliberately added CTAB seemed to inhibit the sorption of positively charged AuNPs. Our experimental results suggest that the electrostatic interaction between AuNPs and pyrite is the most critical force in the sorption process, while competitive sorption exists between CTAB and CTAB-capped AuNPs. Solution parameters such as pH, ionic strength, and ligand concentration are demonstrated to play a substantial role in the above sorption mechanism and can thus jointly control the sorption and aggregation

behaviors of AuNPs. Combined with previous studies, our new findings may provide important constraints to the metallogenic mechanism of certain AuNPs-containing ore deposits, especially when evaluating the validity of the long standing colloidal transport theory. In addition, insights from our study may also be applicable to many natural environments, where NPs may encounter minerals in the presence of abundant organic molecules. For example, in such systems, organic ligands can not only stabilize NPs against aggregation through electrostatic repulsion, but also compete against NPs for sorption sites on mineral surfaces.

Supplementary Materials: The following are available online at http://www.mdpi.com/2075-163X/8/10/428/s1, Figure S1: XRD of pyrite; Figure S2: SEM micrographs of synthesized pyrite; Figure S3: Effect of ageing on the stability of positively charged AuNPs; Figure S4: Au 4f XPS spectrum of pyrite after sorption of positively charged AuNPs; Figure S5: zeta potential of pyrite at different NaCl concentrations (pH = 4); Figure S6: zeta potential of pyrite at different NaCl concentrations (pH = 7); Figure S7: zeta potential of positively charged Au NPs at different NaCl concentrations (pH = 4); Figure S8: zeta potential of positively charged Au NPs at different NaCl concentrations (pH = 7).

Author Contributions: Q.W. proposed the research direction and guided the project; S.L. performed the experiment and wrote this manuscript; X.N. analyzed the data; M.Y. discussed the results; P.Z. joined the discussion of data; Y.F. provided some useful suggestions.

Funding: This work was supported by the Chinese Academy of Sciences ("Hundred Talents Program"), the National Natural Science Foundation of China (41173074), Guizhou Provincial Science and Technology projects ([2018]1172), The Special Key Laboratory of Material Electrochemistry of Guizhou Province (2018-04), and Doctoral Research Startup Project in 2016 of Guizhou Normal University in China.

Conflicts of Interest: The authors declare no conflict of interest.

References

1. Hochella, M.F.; Lower, S.K.; Maurice, P.A.; Penn, R.L.; Sahai, N.; Sparks, D.L.; Twining, B.S. Nanominerals, mineral nanoparticles, and earth systems. *Science* **2008**, *319*, 1631–1635. [CrossRef] [PubMed]
2. Trun, L.; Bañares, M.A. *Advances in Experimental Medicine and Biology*; Cohen, I.R., Ed.; Springer: Berlin/Heidelberg, Germany, 2016; pp. 1–360.
3. Kelle, A.A.; McFerran, S.; Lazareva, A.; Suh, S. Global life cycle releases of engineered nanomaterials. *J. Nanopart. Res.* **2013**, *15*, 1692–1708. [CrossRef]
4. Fenter, P.; Sturchio, N.C. Mineral-water interfacial structures revealed by synchrotron X-ray scattering. *Prog. Surf. Sci.* **2004**, *77*, 171–258. [CrossRef]
5. Stumm, W. *Chemistry of the Solid-Water Interface*; John Wiley & Sons, Inc.: Hoboken, NJ, USA, 1992; pp. 1–432.
6. Mikhlin, Y.; Romanchenko, A.; Likhatsk, M.; Karacharov, A.; Erenburg, S.; Trubina, S. Understanding the initial stages of precious metals precipitation: Nanoscale metallic and sulfidic species of gold and silver on pyrite surfaces. *Ore Geol. Rev.* **2011**, *42*, 47–54. [CrossRef]
7. Gupta, G.S.; Senapati, V.A.; Dhawan, A.; Shanker, R. Heteroagglomeration of zinc oxide nanoparticles with clay mineral modulates the bioavailability and toxicity of nanoparticle in Tetrahymena pyriformis. *J. Colloid Interf. Sci.* **2017**, *495*, 9–18. [CrossRef] [PubMed]
8. Smith, B.M.; Pike, D.J.; Kelly, M.O.; Nason, J.A. Quantification of Heteroaggregation between Citrate-Stabilized Gold Nanoparticles and Hematite Colloids. *Environ. Sci. Technol.* **2015**, *49*, 12789–12799. [CrossRef] [PubMed]
9. Chiu, C.W.; Ou, G.B.; Tsai, Y.H.; Lin, J.J. Immobilization of silver nanoparticles on exfoliated mica nanosheets to form highly conductive nanohybrid films. *Nanotechnology* **2015**, *26*. [CrossRef] [PubMed]
10. Park, Y.C.; Paulsen, J.; Nap, R.J.; Whitaker, D.R.; Mathiyazhagan, V.; Song, Y.Q.; HüRlimann, M.; Szleifer, I.; Wong, J.Y. Adsorption of superparamagnetic iron oxide nanoparticles on silica and calcium carbonate sand. *Langmuir* **2014**, *30*, 784–792. [CrossRef] [PubMed]
11. Alex, S.; Tiwari, A. Functionalized gold nanoparticles: Synthesis, properties and applications—A review. *J. Nanosci. Nanotechnol.* **2015**, *15*, 1869–1894. [CrossRef] [PubMed]
12. Tiede, K.; Hassellöv, M.; Breitbarth, E.; Chaudhry, Q.; Boxall, A.B.A. Considerations for environmental fate and ecotoxicity testing to support environmental risk assessments for engineered nanoparticles. *J. Chromatogr. A* **2009**, *1216*, 503–509. [CrossRef] [PubMed]

13. Tiede, K.; Boxall, A.B.A.; Tear, S.P.; Lewis, J.; David, H.; Hassellöv, M. Detection and characterization of engineered nanoparticles in food and the environment. *Food. Addit. Contam.* **2008**, *7*, 795–821. [CrossRef] [PubMed]
14. Wang, Y.F. Nanogeochemistry: Nanostructures, emergent properties and their control on geochemical reactions and mass transfers. *Chem. Geol.* **2014**, *378*, 1–23. [CrossRef]
15. Palenik, C.S.; Utsunomiya, S.; Reich, M.; Kesler, S.E.; Wang, L.; Ewing, R.C. "Invisible" gold revealed: Direct imaging of gold nanoparticles in a Carlin-type deposit. *Am. Mineral.* **2004**, *89*, 1359–1366. [CrossRef]
16. Hough, R.M.; Noble, R.R.P.; Reich, M. Natural gold nanoparticles. *Ore Geol. Rev.* **2011**, *42*, 55–61. [CrossRef]
17. Reich, M.; Kesler, S.E.; Utsunomiya, S.; Palenik, C.S.; Chryssoulis, S.L.; Ewing, R.C. Solubility of gold in arsenian pyrite. *Geochim. Cosmochim. Acta* **2005**, *11*, 2781–2796. [CrossRef]
18. Romanchenko, A.S.; Mikhlin, Y.L.; Makhova, L.V. Investigation of Gold Nanoparticles Immobilized on the Surface of Pyrite by Scanning Probe Microscopy, Scanning Tunneling Spectroscopy, and X-ray photoelectron Spectroscopy. *Glass Phys. Chem.* **2007**, *4*, 417–421. [CrossRef]
19. Muntean, J.L.; Cline, J.S.; Simon, A.C.; Longo, A.A. Magmatic-hydrothermal origin of Nevada's Carlin-type gold deposits. *Nat. Geosci.* **2011**, *4*, 122–127. [CrossRef]
20. Fougerouse, D.; Reddy, S.M.; Saxey, D.W.; Rickard, W.D.A.; Van Riessen, A.; Micklethwaite, S. Nanoscale gold clusters in arsenopyrite controlled by growth rate not concentration: Evidence from atom probe microscopy. *Am. Mineral.* **2016**, *101*, 1916–1919. [CrossRef]
21. Eghbalnia, M. Electrochemical and Raman Investigation of Pyrite and Chalcopyrite Oxidation. Ph.D. Thesis, University of British Columbia, Vancouver, BC, Canada, April 2012. Available online: https://open.library.ubc.ca/cIRcle/collections/ubctheses/24/items/1.0072701 (accessed on 25 September 2018).
22. Chandra, A.P.; Gerson, A.R. The mechanisms of pyrite oxidation and leaching: A fundamental perspective. *Surf. Sci. Rep.* **2010**, *65*, 293–315. [CrossRef]
23. Fu, Y.H.; Nie, X.; Qin, Z.H.; Li, S.S.; Wan, Q. Effect of Particle Size and Pyrite Oxidation on the Sorption of Gold Nanoparticles on the Surface of Pyrite. *J. Nanosci. Nanotechnol.* **2017**, *17*, 6367–6376. [CrossRef]
24. Duan, Y.H.; Han, D.S.; Batchelor, B.; Abdel-Wahab, A. Synthesis, characterization, and application of pyrite for removal of mercur. *Colloid Surf. A* **2016**, *490*, 326–335. [CrossRef]
25. Lau, B.L.T.; Huang, R.X.; Madden, A.S. Electrostatic adsorption of hematite nanoparticles on self-assembled monolayer surfaces. *J. Nanopart. Res.* **2013**, *15*, 1873–1882. [CrossRef]
26. Frens, G. Controlled nucleation for the regulation of the particle size in monodisperse gold suspensions. *Nat. Phys. Sci.* **1973**, *105*, 20–22. [CrossRef]
27. Sau, T.K.; Murphy, S.C. Room Temperature, High-Yield Synthesis of Multiple Shapes of Gold Nanoparticles in Aqueous Solution. *J. Am. Chem. Soc.* **2004**, *126*, 8648–8649. [CrossRef] [PubMed]
28. Wang, J.; Li, Y.F.; Huang, C.Z.; Wu, T. Rapid and selective detection of cysteine based on its induced aggregates of cetyltrimethylammonium bromide capped gold nanoparticles. *Anal. Chim. Acta* **2008**, *626*, 37–43. [CrossRef] [PubMed]
29. Khan, Z.; Singh, T.; Hussain, J.I.; Hashmi, A.A. Au(III)-CTAB reduction by ascorbic acid: Preparation and characterization of gold nanoparticles. *Colloid Surf. B* **2013**, *104*, 11–17. [CrossRef] [PubMed]
30. Yang, Z.T.; Liu, X.J.; Feng, X.L.; Cui, Y.X.; Yang, X.W. Hydrothermal synthesized micro/nano-sized pyrite used as cathode material to improve the electrochemical performance of thermal battery. *J. Appl. Electrochem.* **2014**, *44*, 1075–1080. [CrossRef]
31. Descostes, M.; Vitorge, P.; Beaucaire, C. Pyrite dissolution in acidic medi. *Geochim. Cosmochim. Acta* **2004**, *22*, 4559–4569. [CrossRef]
32. Feng, B.; Lu, Y.P.; Luo, X.P. The effect of quartz on the flotation of pyrite depressed by serpentine. *J. Mater. Res. Technol.* **2015**, *4*, 8–13. [CrossRef]
33. Hu, X.M.; Yang, S.S. Spectrophotometric method for determination of cetyltrimethyl-ammonium bromide in water. *Adm. Technol. Environ. Monit.* **2010**, *5*, 45–47.
34. Badawy, A.M.E.; Luxton, T.P.; Silva, R.G.; Scheckel, K.G.; Suidan, M.T. Impact of environmental conditions (pH, ionic strength, and electrolyte type) on the surface charge and aggregation of silver nanoparticles suspensions. *Environ. Sci. Technol.* **2010**, *44*, 1260–1266. [CrossRef] [PubMed]
35. Lide, D.R. *CRC Handbook of Chemistry and Physics*; Taylor and Francis Boca Raton FL: Boca Raton, FL, USA, 2007; pp. 1–2560.

36. Hamon, C.; Bizien, T.; Artzner, F.; Even-Hernandez, P.; Marchi, V. Replacement of CTAB with peptidic ligands at the surface of gold nanorods and their self-assembling properties. *J. Colloid Interface Sci.* **2014**, *424*, 90–97. [CrossRef] [PubMed]
37. Kosmulski, M. *Surface Charging and Points of Zero Charge*; Kosmulski, M., Ed.; Taylor and Francis Boca Raton FL: Boca Raton, FL, USA, 2009; pp. 1–1094.
38. Fornasiero, D.; Eijt, V.; Ralston, J. An electrokinetic study of pyrite oxidation. *Colloids Surfaces* **1992**, *62*, 63–73. [CrossRef]
39. Monfared, A.D.; Ghazanfari, M.H.; Jamialahmadi, M.; Helalizadeh, A. Adsorption of silica nanoparticles onto calcite: Equilibrium, kinetic, thermodynamic and DLVO analysis. *Chem. Eng. J.* **2015**, *281*, 334–344. [CrossRef]
40. Peng, C.; Zhang, W.; Gao, H.P.; Li, Y.; Tong, X.; Li, K.G.; Zhu, X.S.; Wang, Y.X.; Chen, Y.S. Behavior and potential impacts of metal-based engineered nanoparticles in aquatic environments. *Nanomaterials* **2017**, *7*, 21. [CrossRef] [PubMed]
41. Johnson, C.A.; Lenhoff, A.M. Adsorption of charged latex particles on mica studied by atomic force microscopy. *J. Colloid Interface Sci.* **1996**, *179*, 587–599. [CrossRef]
42. Sadowska, M.; Adamczyk, Z.; Nattich-Rak, M. Mechanism of nanoparticle deposition on polystyrene latex particles. *Langmuir* **2014**, *30*, 692–699. [CrossRef] [PubMed]